New measurements of photoneutron spectra investigating specific signatures of carbon, nitrogen, and oxygen

Clement Besnard Vauterin, Benjamin Rapp, Valentin Blideanu

New Measurements of Photoneutron Spectra investigating specific signatures of Carbon, Nitrogen, and Oxygen

C. Besnard-Vauterin[1*], B. Rapp[1], and V. Blideanu[1]

[1]Université Paris-Saclay, CEA, List, Laboratoire National Henri Becquerel (LNE-LNHB)
F-91129, Palaiseau, France

clement.besnardvauterin@cea.fr, benjamin.rapp@cea.fr, valentin.blideanu@cea.fr

ABSTRACT

We report new measurements on photoneutron spectra from graphite, glucose, and melamine, revealing distinct signatures corresponding to carbon, oxygen, and nitrogen individual elements. Using a 23-MV electron linear accelerator (LINAC) and EJ-309 liquid scintillators with advanced pulse shape discrimination and pile-up rejection algorithms, we successfully detected fast neutrons from photo-nuclear (γ,Xn) reactions within an intense pulsed photon field. Energy deposition from fast neutrons was unfolded using two well-known independent algorithms ML-EM and GRAVEL. Our findings indicate discrepancies between the experimental results and Monte-Carlo simulations performed with the widely-used code MCNP6, highlighting the need for new data in order to improve the models used for the simulation of photoneutron production. These results have significant implications for various nuclear physics applications, including electron accelerator facilities decommissioning, illicit material detection for homeland security, and global radiotherapy patient dosimetry including neutron dose.

KEYWORDS: Neutron Spectrometry, Organic Scintillator, LINAC, Giant Dipole Resonance, Monte-Carlo Simulations

I. INTRODUCTION

Photoneutron energy spectra, especially those produced in reactions on light elements such as carbon, oxygen and nitrogen, remain inadequately characterized, despite their critical importance in various applications as pointed out in a previous work related to Monte-Carlo codes benchmark [1]. Activation and decommissioning of electron accelerator facilities, detection of illicit materials for homeland security and the assessment of neutron doses in radiotherapy treatments are

*Contact author: clement.besnardvauterin@cea.fr

nowadays very actual applications in which the photo-nuclear interactions eventually leading to neutron productions are the dominant process.

In the field of nuclear security, high-energy photon interrogation using linear electron accelerators (LINACs) operating around 9 MeV has played a pivotal role in detecting special nuclear materials and characterizing nuclear waste. However, recent advancements in active photon interrogation techniques above 12 MeV underscore the pressing need for precise photoneutron spectra data [2]. Understanding these spectra—particularly the signatures of carbon, nitrogen, and oxygen—is essential, as these elements are key components of materials such as explosives, narcotics, and chemical agents representing significant security threats.

Also, in medical applications photo-nuclear reactions induced by Bremsstrahlung photons in LINAC facilities not only contribute to patient global dosimetry and affect accelerator components but also influence facility decommissioning and radioactive waste management [3]. Regulatory authorities and waste-management operators increasingly demand accurate characterization of generated radioactive waste to ensure appropriate management strategies.

Despite the crucial importance of photoneutron spectra, existing data are sparse and outdated, limiting the accuracy of Monte-Carlo simulations in modelling these interactions. The absence of precise experimental measurements hampers the development of reliable predictive models for photoneutron production for applications simulations.

To address these challenges, this study presents novel measurements of photoneutron energy spectra from light-element targets established for the first time by proton recoil detection. By employing a 23-MV electron LINAC and EJ-309 liquid organic scintillators with advanced pulse shape discrimination and pile-up rejection algorithms, we unfold and analyse the photoneutron energy spectra from graphite (C), glucose ($C_6H_{12}O_6$), and melamine ($C_3H_6N_6$) targets. These targets, chosen for their carbon, oxygen, and nitrogen content, serve as benchmark for investigating photo-nuclear interactions, particularly within the giant dipole resonance (GDR) region.

II. EXPERIMENTAL PROCEDURE

A. Photon source based on a medical linear electron accelerator

The measurements were performed using a Varian TrueBeam medical linear electron accelerator at the Doseo platform of CEA in Saclay (France). This accelerator primarily designed for radiotherapy applications, operates with a maximal energy estimated at 22.9 ± 0.7 MeV. Modifications detailed in Ref. [4] were applied to optimize the accelerator's operating regime to fulfil our specific experimental needs. The accelerated electron beam interacts with an internal electron-to-photon conversion target inside the accelerator head producing Bremsstrahlung photons as shown on Figure 1. The photon field, characterized by a typical Bremsstrahlung spectrum with a maximum energy of 23.6 MeV, spans an area of 40 × 40 cm^2 measured at one

meter from the exit of the accelerator's vacuum section. The accelerator produces electron pulses lasting 3–4 μs, with a pulse frequency ranging from a few to 360 Hz.

B. Neutron detector set-up and data acquisition

The neutron measurements were carried out using two organic liquid scintillators (EJ-309), housed in cylindrical cells with a diameter and height of 5.08 cm. Each scintillator is mainly composed of xylene (>90%) as the solvent and aromatic fluorine (<10%) as the solute, with a density of 0.964 g/cm³. The EJ-309 scintillators share similarities with well-established detectors such as BC501A, NE213, and EJ-301, offering excellent neutron-photon pulse shape discrimination (PSD) in mixed radiation fields. A key feature of EJ-309 is its fast decay time of 3.2 ns, which is crucial for handling the high photon flux produced during LINAC pulses.

The two detectors were placed inside a detection cell with 30 cm thick walls, constructed from high-density polyethylene (HDPE) to shield against contaminating neutrons from the accelerator. A window facing the irradiated targets allows the detection of photoneutrons without obstruction. Tungsten and lead bricks are included inside the cell to reduce photon flux reaching the detectors in order to minimize their saturation related to the pulsed beam. Monte-Carlo simulations were performed to confirm that the contribution of additional neutrons above 2 MeV produced in the shielding materials was negligible compared to those emitted by the irradiated targets. The detection cell was positioned at an angle of 90° relative to the beam direction to decrease as much as possible its exposure to the main photon beam, which is mainly forward directed.

The detection system uses Hamamatsu R329-02 photomultiplier tubes (PMTs), operated at −950 V, chosen for their fast response time with a 2.6 ns anode pulse rise time. Signal acquisition was managed using a CAEN DT5743 digitizer for each detector, operating at a 3.2 GHz sampling frequency, with an input range of ±1.25 V and 12-bit resolution. The acquisition system was synchronized with an external trigger signal generated by the Varian TrueBeam accelerator, processed through a counter-timer module. This setup allowed precise control of the signal length and delay, ensuring synchronization with the accelerator pulses. An AND gate was applied via CAEN WaveCatcher software to select events occurring within a predefined time window. More details can be found in the previous work described in Ref. [4].

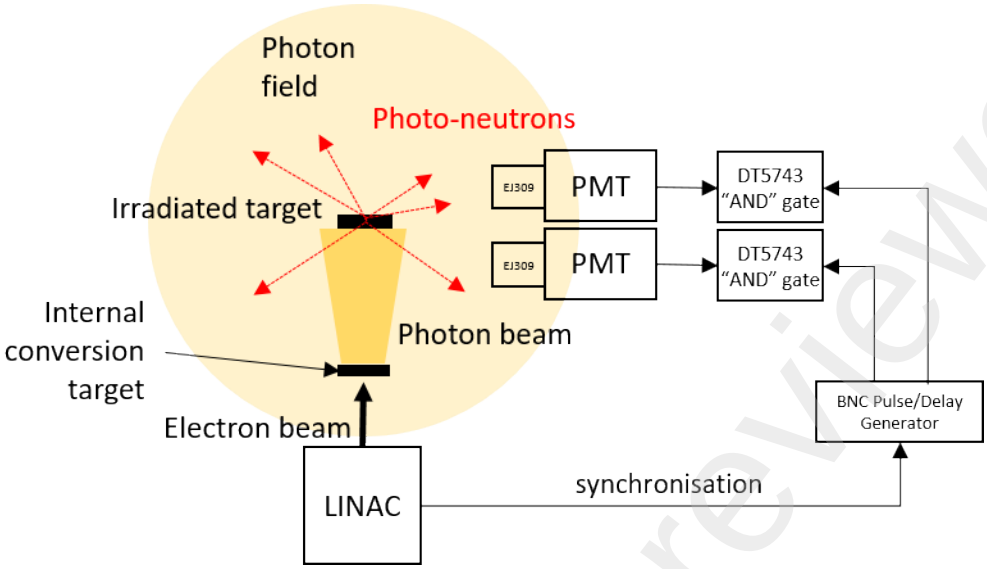

Figure 1. Schematic view of the experimental set-up.

C. Detectors calibration, response function and unfolding methodology

The EJ-309 scintillators were calibrated using both photon sources and mono-energetic neutron beams. Photon calibration involved determining conversion factors from integrated pulses (in V·ns) to MeVee (mega-electron-volt electron equivalent) by analysing the Compton edges corresponding to various photon sources and it was performed twice: first under standard laboratory conditions and then at the Amande neutron beam facility [5]. This allowed to account for the attenuation effect due to the 50-meter cable used during calibration with neutrons and consequently associated correction to be applied.

Neutron calibration further allowed to convert the deposited energy (in MeV) to MeVee, ensuring accurate energy deposition measurements. Figure 2 presents the neutron calibration curve obtained for detectors exposure to mono-energetic neutron beams. Our calibration curve is compared to those for similar liquid scintillator detectors reported in Refs. [6] and [7] demonstrating consistency in the established calibration data.

The response matrix of the detectors was simulated using the Monte-Carlo code Geant4 [8], with the NRESP7 option activated to include multi-step reactions in the scintillating material [9]. This response matrix played a key role in accurately unfolding the photoneutron spectra using two robust algorithms: Maximum Likelihood-Expectation Maximization (ML-EM) [10] and GRAVEL [11], the latter being based on a non-linear iterative least squares method. These algorithms were chosen for their proven effectiveness in extracting true neutron energy spectra from the measured data.

Classical pulse shape discrimination (PSD) techniques based on the charge comparison method (CCM) were applied to distinguish between neutron and photon events. An example of the PSD performance of our method is shown in Figure 3 for the Am-Be source. The FoM (Figure of Merit) value for this example was 1.5 at 1 MeVee.

To further validate our unfolding methodology, we compared our unfolded neutron spectrum for the Am-Be source with the reference one provided by the ISO-8529 standard [12]. Figure 4 illustrates this comparison, highlighting the close agreement and thus confirming both the accuracy and global robustness of our method, particularly in the region of fast neutrons, and the accurate calibration of our detector.

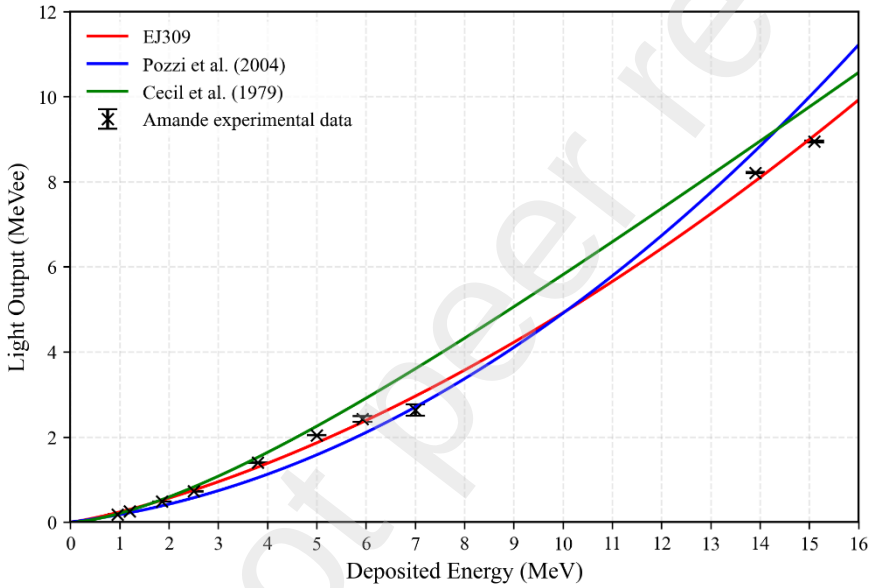

Figure 2: EJ-309 detector calibration curve obtained in this work using mono-energetic neutrons (in red) compared with data from the literature.

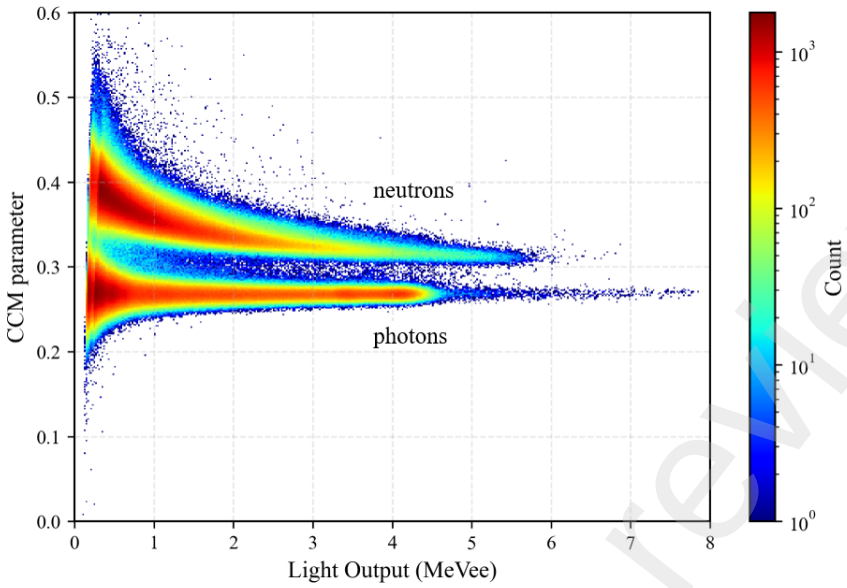

147

148 Figure 3: Pulse shape discrimination scatter-density plot for neutrons and photons obtained with
149 the Am-Be source.

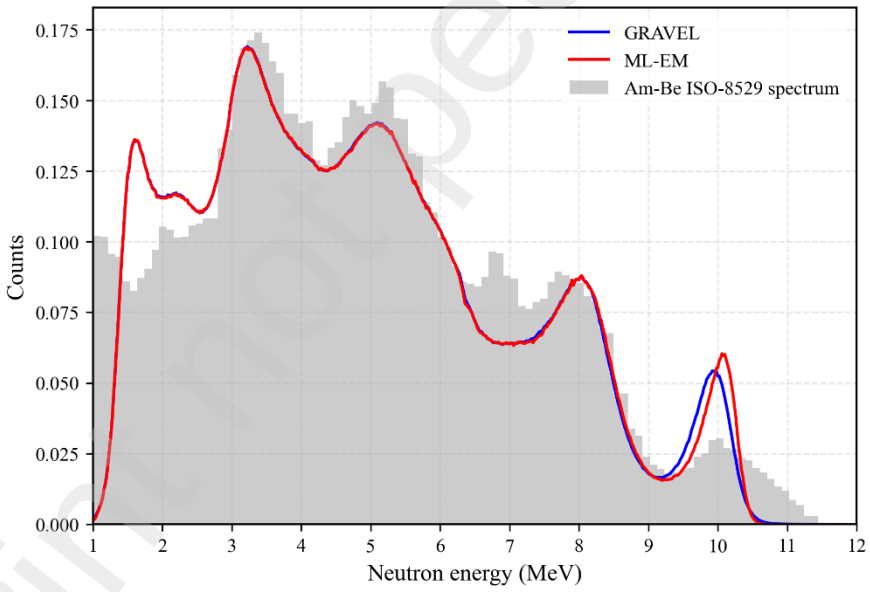

150

151 Figure 4: Comparison between the unfolded Am-Be neutron spectrum obtained in this work using
152 two algorithms (300 iterations each) and the reference values from the ISO-8529 standard
153 (histogram).

154 **D. Target materials**

155 To investigate the photoneutron energy spectra and individual elements signatures, we selected
156 graphite, glucose, and melamine as target materials. Each target was chosen for its elemental
157 composition allowing to provide distinct signatures for carbon, oxygen, and nitrogen. All targets

were irradiated at a distance of 1 meter from the accelerator's exit point, fully exposed to the 40 × 40 cm^2 photon field.

1. Graphite target

The graphite target, with the chemical formula C, was used to study carbon signatures. It consisted of a solid block with dimensions of 30 × 30 × 30 cm^3. The homogeneous, high-density nature of graphite makes it an ideal candidate for photoneutron studies involving carbon.

2. Glucose target

The glucose target, with the chemical formula $C_6H_{12}O_6$ was chosen to explore oxygen signatures. This target was in powder form with a total mass of 10 kg contained by a bucket with 1 mm-thick plastic walls, enough to ensure uniform irradiation and target integrity during the experiment while minimizing any additional photoneutron production.

3. Melamine target

The melamine target, with the chemical formula $C_3H_6N_6$, was selected to investigate nitrogen signatures. As for the glucose target, melamine in powder form with a total mass of 10 kg was housed in a bucket of the same type.

III. RESULTS AND DISCUSSION

A. Photoneutron spectra from irradiation of graphite, glucose, and melamine targets

PSD results for both detectors are cumulated in a single scatter density plot after applying the appropriate calibration to both individual detectors. The method for selecting neutron pulses to construct the recoil proton spectrum and unfold it to obtain the neutron spectrum was the one previously described in the subsection II.C. An example of scatter density plot for the melamine target is given in Figure 5. The FoM value achieved here was 1.25 at 1 MeVee demonstrating the effectiveness of traditional PSD methods even when dealing with complex experimental conditions specific to electron accelerators, characterized by pulsed and mixed neutron/photon radiation fields with high photon fluxes. The corresponding photoneutron spectra obtained from the graphite, glucose, and melamine targets are presented in Figures 6, 7, and 8, respectively.

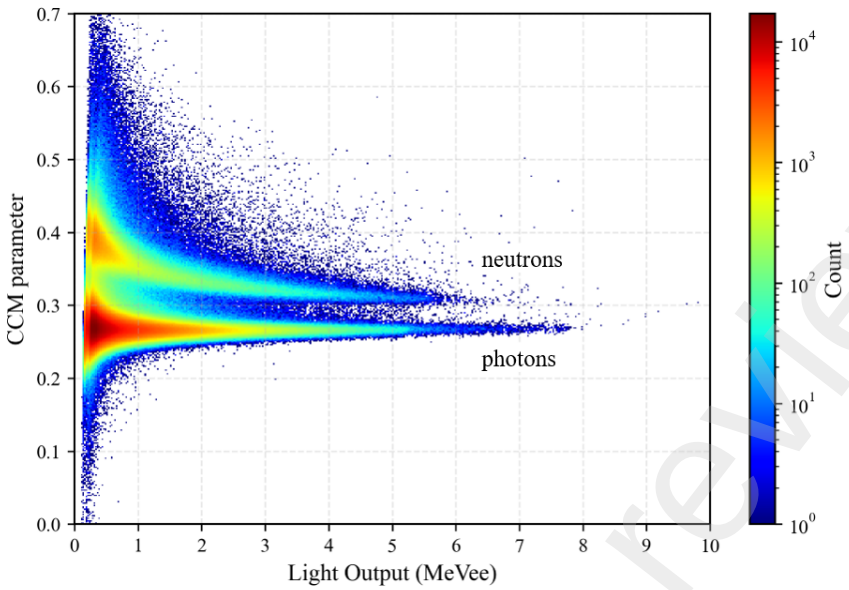

Figure 5: Pulse shape discrimination scatter-density plot for neutrons and photons for the melamine target irradiation.

The solid lines shown in these figures correspond to the average values of the spectra unfolded with the two algorithms ML-EM and GRAVEL. The shaded area, mainly visible at high energies in the spectrum from the melamine target, is determined as the difference between these two spectra.

Neutron energy distributions resulting from (γ,Xn) reactions on each target material were so determined experimentally. As it will be discussed in the next section, their detailed analysis subsequently allows the identification of specific signatures corresponding to the individual elements carbon, oxygen, and nitrogen. As expected according to the composition of the respective target materials irradiated, the graphite target primarily highlights the carbon specific signatures, while the glucose target reveals oxygen signatures and the melamine target exhibits signatures from nitrogen.

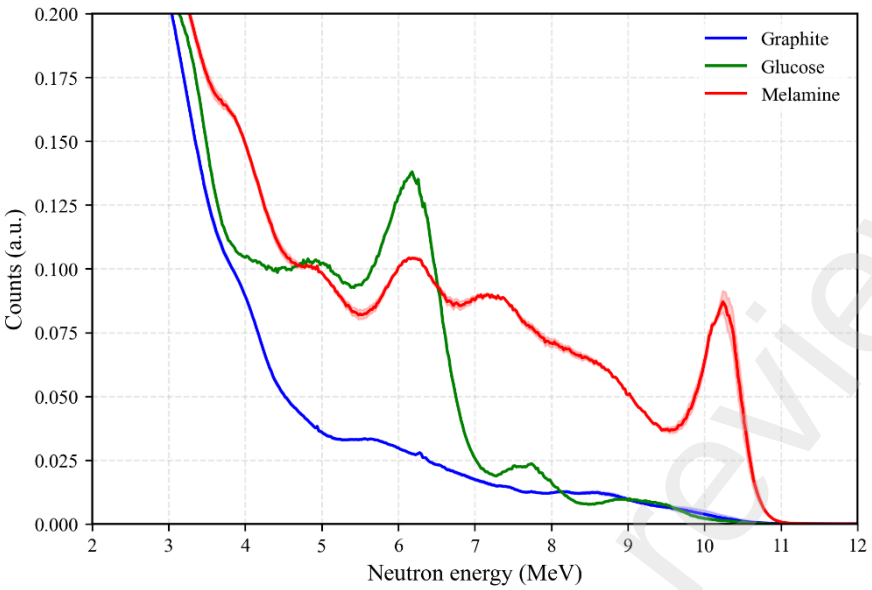

Figure 6: Experimental photoneutron spectra from the irradiation of the graphite, glucose and melamine targets.

B. Carbon specific signature in the photoneutron spectrum from graphite target

The neutron spectrum measured with the carbon target (blue curve in Figure 6) is not background-subtracted, as it almost corresponds to the photoneutron background from the surrounding environment (including contributions from the accelerator, detector shielding, and the bunker). This is due to the fact that carbon from the target emits very few photoneutrons since the Q-value of the $^{12}C(\gamma,n)^{11}C$ reaction is very high at −18.7217 MeV and so its threshold is only slightly below the highest energy (23.6 MeV) of photons produced by the accelerator during our experiments.

Monte-Carlo simulations using the MCNP6.2 code reproducing the experimental configuration were performed allowing to calculate the contributions from photo-nuclear reactions on ^{12}C and ^{13}C separately as shown in the resulting spectra given in Figure 7. It must be reminded that ^{13}C accounts for approximately 1.1% in the graphite natural composition which explains its lower contribution to the total photoneutron production. The contribution from ^{12}C has a maximum slightly below 3 MeV, the photoneutron emission probability rapidly decreasing afterwards. Around 5 MeV the contribution from ^{13}C becomes dominant, resulting in a noticeable change in the spectral slope. This change is consistent with the experimental spectrum for the carbon target from Figure 6, where a similar change in the shape of the photoneutron energy distribution is observed around the same energy.

This behaviour is explained by the reaction kinematics, since the maximum electron energy from our accelerator is 23.6 MeV and so is the maximum energy of the photons it produces and being used for the irradiations performed in this work. This limits the maximum possible photoneutron

energy from $^{12}C(\gamma,n)^{11}C$ reaction to 4.9 MeV, considering the photo-nuclear reaction threshold as discussed above. This corresponds to the energy value at which the slope change is observed in the measured photoneutron spectrum. The more energetic neutrons can thus only be produced by photo-nuclear reactions on ^{13}C, since in this case the Q-value is much lower at −4.9463 MeV. The photoneutron distribution from this later reaction extends up to 10 MeV, although even more energetic neutrons can theoretically be emitted but they were not evidenced experimentally by our measurements.

The overall shape of the simulated spectrum is in agreement with the theoretical one $\sigma(\gamma,n)I(E_\gamma, 23)$ shown in Figure 9. The later was deduced by folding the Bremsstrahlung spectrum $I(E_\gamma, 23)$ for a 23 MeV electron beam corresponding to our accelerator with the experimental $\sigma(\gamma,n)$ cross-section values from Cook et al. [13]. The agreement found confirm that the photoneutron emission process is occurring as expected, predominantly leaving the ^{11}C residual nucleus in its ground state (Figure 8).

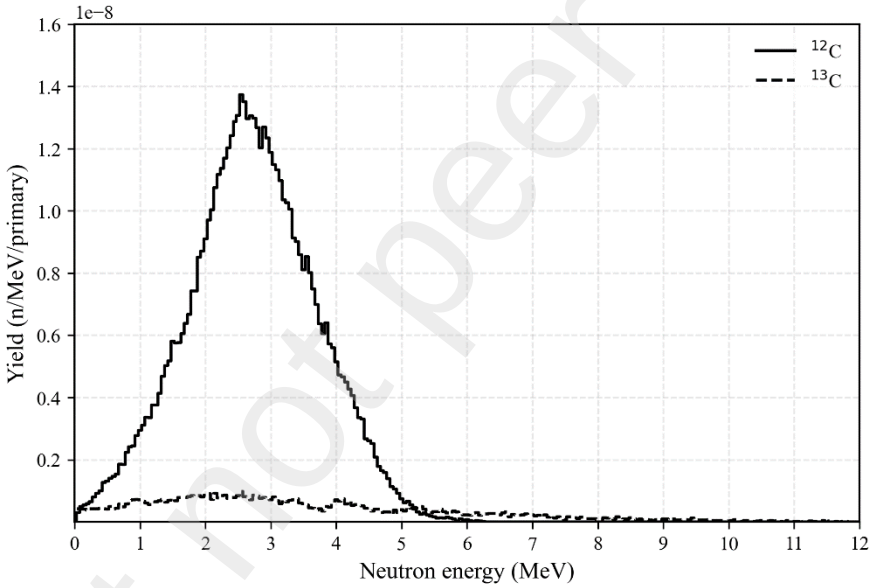

Figure 7: MCNP6.2 simulated photoneutron spectrum for graphite irradiation with the Bremsstrahlung photons corresponding to our accelerator.

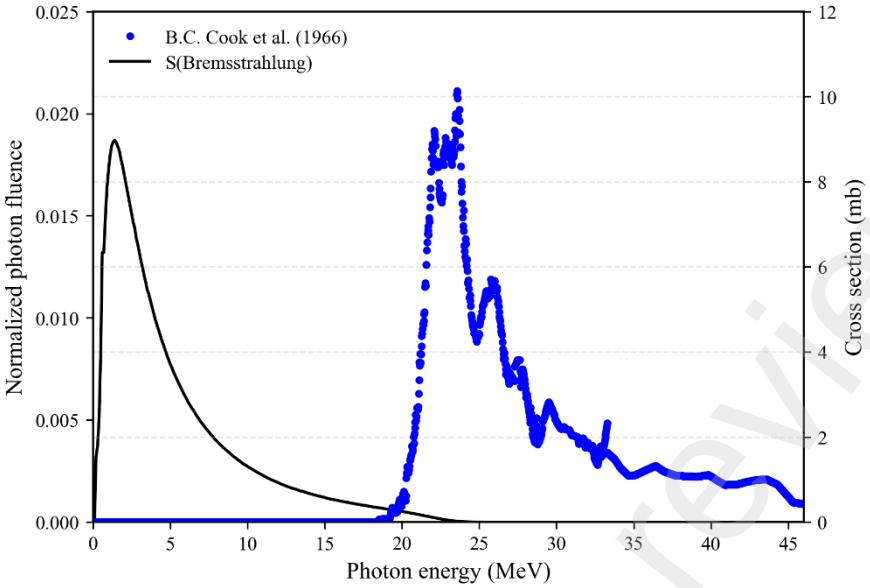

Figure 8: Experimental cross-sections from Cook et al. [13] and the Bremsstrahlung spectrum $I($ $E_\gamma, 23)$ produced by the 23.6 MeV electron beam from our accelerator.

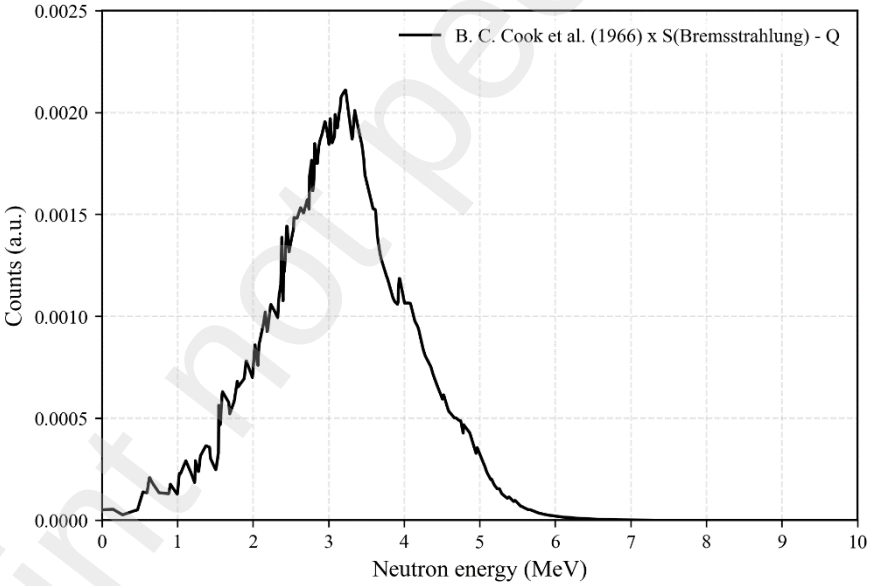

Figure 9: Calculated theoretical photoneutron spectrum $\sigma(\gamma,n)I(E_\gamma, 23)$ corresponding to ^{11}C residual nucleus in its ground state.

C. Oxygen specific signature in the photoneutron spectrum from glucose target

The level density of ^{16}O is relatively low because it is a doubly magic nucleus. In the ^{16}O(γ,n) reaction, the residual nucleus ^{15}O also has a low level density, with its first excited state appearing at 5.183 MeV [14]. The emission of one neutron in the $(\gamma$,n) photo-nuclear reaction will leave the resulting residual nucleus ^{15}O either in its ground state or in an excited state.

To isolate the contribution of photo-nuclear reactions on oxygen from the total spectrum measured during glucose irradiation, we subtracted from it the spectrum obtained from the irradiation of the graphite target presented in the previous section. As it has been discussed, few neutrons from this spectrum are produced by photo-nuclear reactions on carbon but most of them are representing the background present in the experimental hall during the irradiations. The resulting spectrum is given in Figure 10 and allows to reveal the distinct signatures of the oxygen present in glucose, namely 3 peaks at 3.5, 5 and 6 MeV respectively.

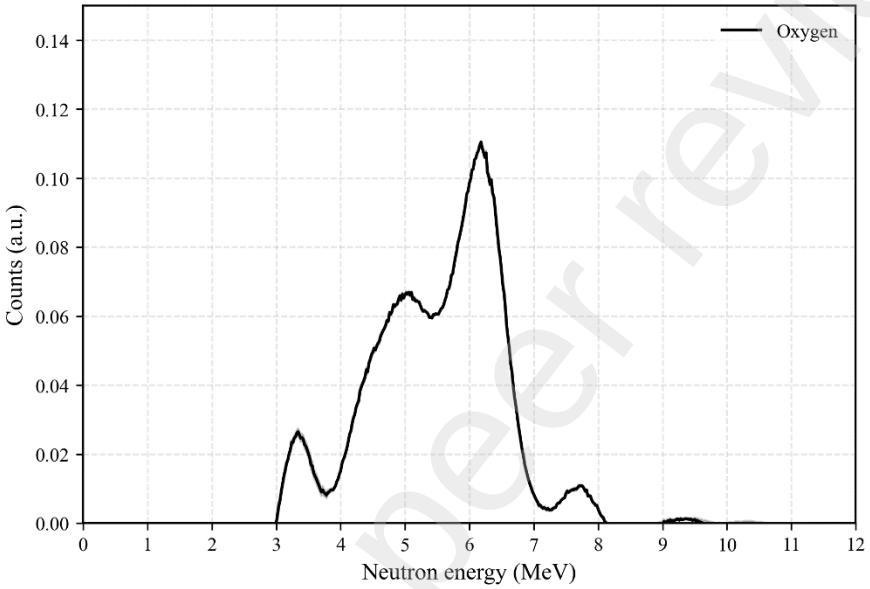

Figure 10: Experimental photoneutron spectrum from photo-nuclear reactions on oxygen.

Previous measurements of photoneutron spectra from ^{16}O were conducted in 1970 as described in Ref. [15] using time-of-flight technique. One of the irradiations, performed with a Bremsstrahlung spectrum with endpoint energy of 22.6 MeV, is sufficiently close to our experimental conditions to allow a direct comparison. The previously measured neutron spectrum at an angle of 82° exhibits notable structures between 3 and 4 MeV and pronounced peaks at 5 MeV and 6 MeV, features that align closely with the experimental results reported in this work obtained using a completely different detection technique based on proton recoil in scintillators. However, an additional peak just below 2 MeV has also been reported but it is not confirmed by our data. This discrepancy is likely due to the challenges associated with background subtraction in our experimental set-up.

The MCNP6.2 simulated photoneutron spectrum for natural oxygen is shown in Figure 11. The photoneutron production is almost exclusively associated to reactions on ^{16}O representing 99.7% in oxygen natural isotopic composition. As in the case of carbon, the simulations agree well with the theoretical spectrum $\sigma(\gamma,n)I(E_\gamma, 23)$ shown in Figure 12 and determined based on the experimental $\sigma(\gamma,n)$ cross-sections from B.C. Cook et al. [16]. This agreement indicates that the

photoneutron emission predominantly leave the ^{15}O residual nucleus in its ground state. It is worth noting that the structures present in the simulated spectrum are also globally confirmed by the measurements reported in this work, except for the peak in the simulated spectrum below 2 MeV which is not observed in our data due to background subtraction limitations.

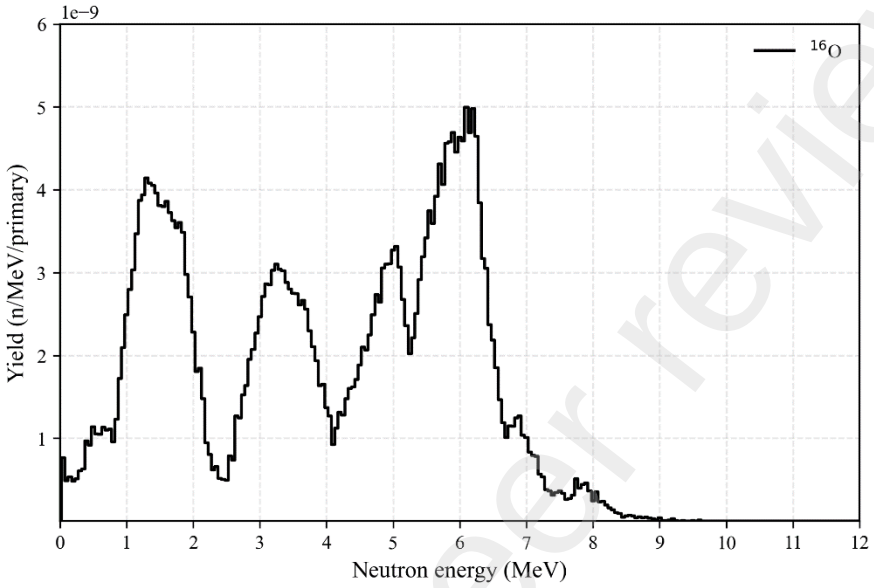

Figure 11: MCNP6.2 simulated photoneutron spectrum for oxygen irradiation with the Bremsstrahlung photons corresponding to our accelerator.

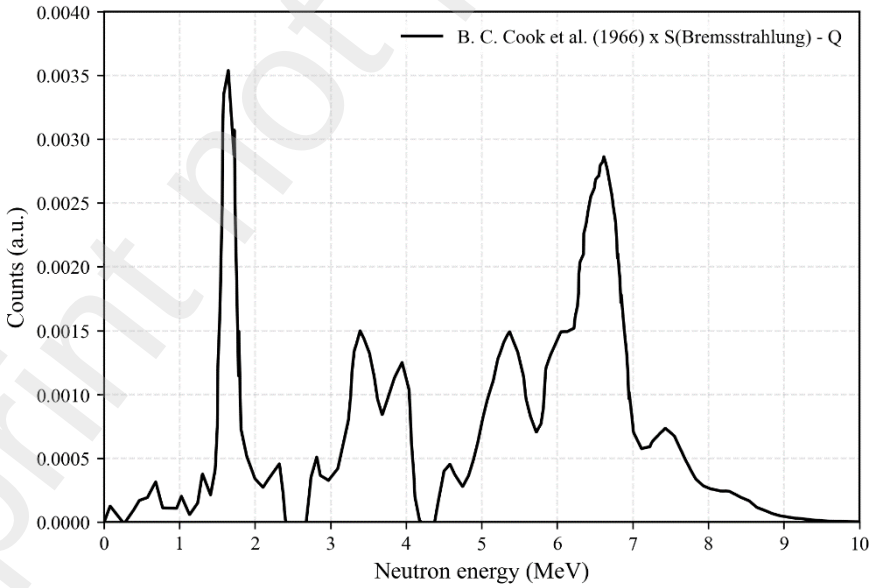

Figure 12: Calculated theoretical photoneutron spectrum $\sigma(\gamma,n)I(E_\gamma, 23)$ corresponding to ^{15}O residual nucleus in its ground state.

D Nitrogen specific signature in the photoneutron spectrum from melamine target

Melamine being made of hydrogen, carbon and nitrogen, the nitrogen specific signature in the total measured photoneutron spectrum can also be isolated by subtracting the carbon contribution. The results presented in Figure 13 reveal distinctive features in the spectrum, several peaks being observed at energies of 1.9, 2.6, 4, 5, 6.3, 7.5 and 10.5 MeV respectively.

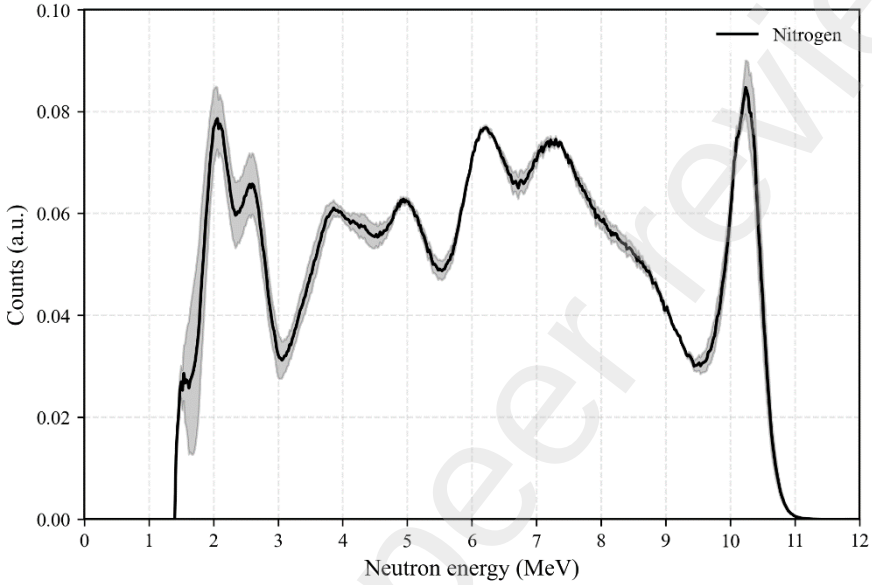

Figure 13: Experimental photoneutron spectrum from photo-nuclear reactions on nitrogen.

Historically, there have been very limited measurements of the photoneutron spectrum for nitrogen. One notable study conducted by the National Research Council of Canada in the 1970s used the time-of-flight method, as described in Refs. [17] and [18]. The reported results shown in Figure 14 involved irradiating liquid nitrogen with Bremsstrahlung photons at endpoint energies of 29.5, 27.5, 23.5, and 21.5 MeV. Despite the very different experimental approach used for the photoneutron measurements, our results confirm most of the previously reported structures in the nitrogen spectrum including peaks at 1.9 MeV and 2.6 MeV and a broader structure at 6.3 MeV. Moreover, these structures were explained by the authors as being associated to a particular two-step photo-nuclear reaction namely $^{14}N(\gamma,p)^{13}C^* \rightarrow {}^{12}C + n$, leading first to the excitation by the incident photons of the ^{14}N nucleus and the emission of a proton, followed by the deexcitation of the remaining ^{13}C left in an excited state (at 7.55 MeV or 11.8 MeV) by the emission of a neutron. Energy conservation allows to calculate the energy of photoneutrons emitted through these mechanisms at around 3 and 4 MeV respectively for the two excited states of ^{13}C. This assessment implies that the photoneutron energy is not influenced by the spectrum of the primary incident photons, which can be assumed to be true as the reactions involved occur through an excitation-deexcitation process in which the memory of the entry channel is typically almost completely lost.

Finally, the two remaining structures observed at the highest photoneutron energies (7.5 and 10.5 MeV) can be attributed to the direct photo-nuclear $^{14}N(\gamma,n)$ reactions leaving the residual ^{13}N in the 3.51 MeV excited state and the ground state respectively.

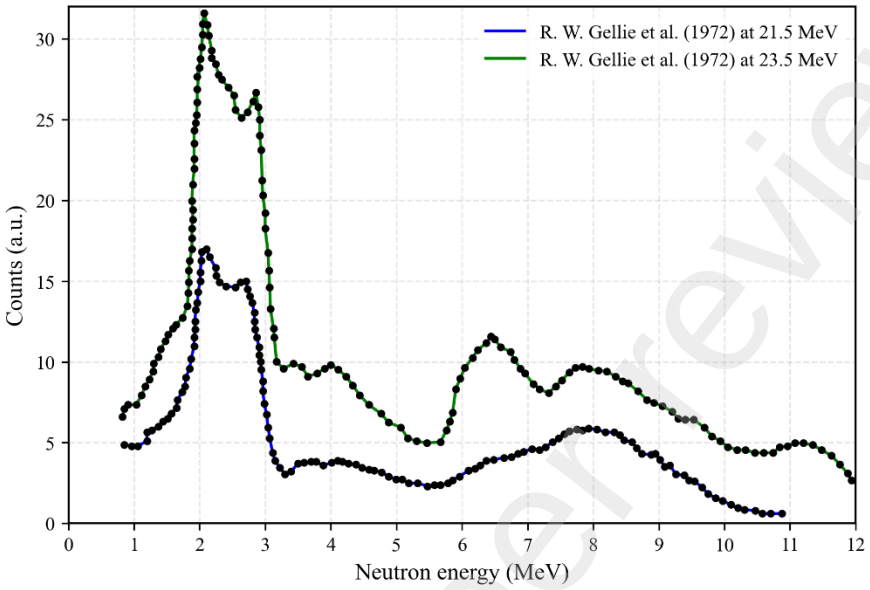

Figure 14: Photoneutron energy distributions from reactions on ^{14}N measured by R. W. Gellie et al. [17] by time-of-flight.

Monte-Carlo simulations were performed using MCNP6.2 with a target of natural nitrogen (99.6% ^{14}N and 0.4% ^{15}N). The simulation results, shown in Figure 15, reveal some similarities to the measured spectrum, including a peak at 3.8 MeV, a broader structure between 6 and 7 MeV and some others at lower energies. However, discrepancies are observed between the simulated and experimental spectra suggesting the inaccuracy of the simulation, particularly consisting in energies of the structures being shifted. This could be explained by an artificial inclusion in the cross-section libraries used by MCNP6 of the photo-nuclear reactions, considering both direct (γ,n) and wo-step (γ,pn) channels, probably based only on better fitting the experimental cross-section values. Indeed, as it can be seen in Figure 16, MCNP6 simulations are able to reproduce accurately the total photoneutron production cross-section showing a very good agreement with the data from Ref. [19] concerning inclusive (γ,Xn) reactions, while being significantly higher than the data from Ref. [20] which are limited to the single contribution of the (γ,n) reaction. The disagreement found however when comparing the simulated energy distribution with the data reported in this work and in Ref. [17] suggest that the above-discussed physics related to the (γ,pn) reaction is not properly implemented in the code.

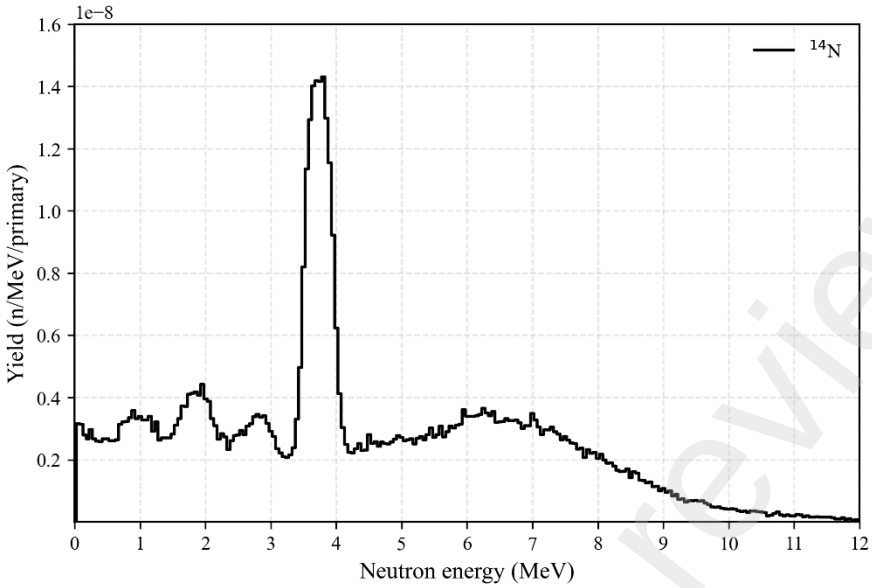

Figure 15: MCNP6.2 simulated photoneutron spectrum for nitrogen irradiation with the Bremsstrahlung photons corresponding to our accelerator.

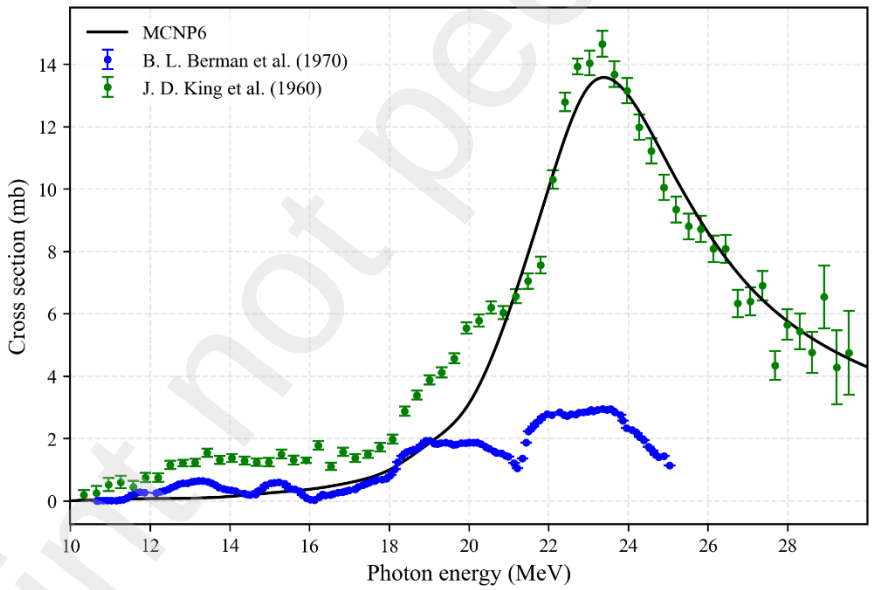

Figure 16: Neutron production cross-sections for photo-nuclear reactions on ^{14}N calculated by MCNP6.2 and compared to the data from References [19] and [20] for (γ,Xn) and (γ,n) reactions respectively.

IV. CONCLUSIONS

We report in this paper the first measurements of neutron spectra from photo-nuclear reactions on graphite, glucose, and melamine performed using proton recoil scintillators, as opposed to former

studies based on time-of-flight methods. By employing a photon source based on a 23-MV linear electron accelerator and advanced EJ-309 liquid scintillators, we successfully detected and analysed fast neutrons from (γ,Xn) reactions on materials of interest for several actual applications such as detection of illicit materials, radiotherapy treatments and induced activation for decommissioning of electron accelerator facilities. This approach allowed the identification in the detailed spectra of distinct signatures of carbon, oxygen, and nitrogen from the photo-nuclear reactions in the giant dipole resonance energy region.

Our experimental results reveal unambiguous photoneutron signatures for each target material. The graphite spectrum predominantly highlight carbon signatures, with contributions from both ^{12}C and ^{13}C. The glucose and melamine photoneutron spectra exhibit in addition respectively the oxygen and nitrogen signatures. These measurements provide valuable insights into the photoneutron emission characteristics from reactions on light elements and represent a significant advancement in improving the experimental techniques in this field.

The comparison between our experimental data and Monte-Carlo simulations with MCNP6.2 code highlighted notable discrepancies in the case of nitrogen, indicating limitations in current cross-section libraries used by the code. This emphasizes the need for improved models and data libraries to enhance the accuracy of simulations for photoneutron production in the reactions on light elements. This work allowed the identification of specific areas to be addressed for further investigation and refinement in simulation practices, aiming to ensure more consistent agreement with experimental data across different elements and conditions.

In the case of oxygen on the other hand the simulations are in good agreement with our data and with measurements from previous studies, providing evidence for the reliability of our experimental approach.

Overall, this study marks a significant advancement by providing new data on photoneutron spectra measured with an original method using proton recoil scintillators. The improved characterization of these spectra from the point of view of photo-nuclear reactions physics is crucial for their better implementation in simulation tools, and by such and through specific applications, for the refinement of nuclear security measures, for the optimization of radiotherapy procedures and more generally for the increase of the reliability of simulations involving photoneutrons. Future work should focus on addressing the identified discrepancies and expanding experimental data to further advancements in this field.

V. ACKNOWLEDGMENTS

Authors would like to acknowledge the financial support provided by the French National Laboratory of Metrology and Testing.

404
405

VI. REFERENCES

[1] V. Blideanu, C. Besnard-Vauterin, D. Horváth, B. Lefebvre, F. Salvat-Pujol and R. Versaci, "Neutron spectra from photonuclear reactions: Performance testing of Monte-Carlo particle transport simulation codes," *Nuclear Instruments and Methods in Physics Research Section B: Beam Interactions with Materials and Atoms,* vol. 549, p. 165292, 2024,.

[2] C. Besnard-Vauterin, V. Blideanu and B. Rapp, "Development of a new method for the detection of illicit materials based on the active interrogation method and photoneutron spectrometry," in *Proc. of 8th International Conference on Advancements in Nuclear Instrumentation, Measurement Methods and their Applications*, Lucca, Italy, 2023.

[3] V. Blideanu, R. Behal, C. Besnard-Vauterin, V. Glagolev, X. Ledoux, J. Mrazek, B. Rapp and E. Simeckova, "Experimental assessment and analysis of calculations accuracy for the neutron-induced radio-isotopes in copper parts of radiotherapy accelerators," *Nuclear Instruments and Methods in Physics Research Section B: Beam Interactions with Materials and Atoms,* vol. 557, p. 165553, 2024.

[4] C. Besnard-Vauterin, B. Rapp and V. Blideanu, "Neutron detection in mixed short-pulsed fields with intense photon flashes for LINAC-based active interrogation applications," *Nuclear Instruments and Methods in Physics Research Section A: Accelerators, Spectrometers, Detectors and Associated Equipment,* vol. 1064, no. 2, p. 169403, 2024.

[5] Institut de Radioprotection et de Sûreté Nucléaire (IRSN), "Monoenergetic neutron fields AMANDE facility," 2024. [Online]. Available: https://en.irsn.fr/research/monoenergetic-neutron-fields-amande-facility. [Accessed 13 09 2024].

[6] S. A. Pozzi, Mullens, J. A. and J. T. Mihalczo, "Analysis of neutron and photon detection position for the calibration of plastic (BC-420) and liquid (BC-501) scintillators," *Nuclear Instruments and Methods in Physics Research Section A: Accelerators, Spectrometers, Detectors and Associated Equipment,* vol. 524, no. 1-3, pp. 92-101, 2004.

[7] R. Cecil, B. Anderson and R. Madey, "Improved predections of neutron detection efficiency for hydrocarbon scintillators from 1 MeV to about 300 MeV," *Nuclear Instruments and Methods,* vol. 161, no. 3, pp. 439-447, 1979.

[8] S. Agostinelli, J. Allison, K. Amako, J. Apostolakis, P. Arce, M. Asai, D. Axen, S. Banerjee, G. Barrand, F. Behner, L. Bellagamba, J. Boudreau, L. Broglia, A. Brunengo, H. Burkhardt, S. Chauvie, J. Chuma, R. Chytracek, G. Cooperman, et. al., "Geant4—a simulation toolkit," *Nuclear Instruments and Methods in Physics Research Section A: Accelerators, Spectrometers, Detectors and Associated Equipment,* vol. 506, pp. 250-303, 2003.

[9] A. Garcia, E. Mendoza, D. Cano-Ott, R. Nolte, T. Martinez, A. Algora, J. Tain, K. Banerjee and C. Bhattacharya, "New physics model in GEANT4 for the simulation of neutron interactions with organic scintillation detectors," *Nuclear Instruments and Methods in Physics Research Section A: Accelerators, Spectrometers, Detectors and Associated Equipment,* vol. 868, pp. 73-81, 2017.

[10] A. P. Dempster, N. M. Laird and D. B. Rubin, "Maximum Likelihood from Incomplete Data via the EM Algorithm," *Journal of the Royal Statistical Society Series B (Methodological),* vol. 39, no. 1, pp. 1-38, 1977.

[11] M. Matzke and K. Weise, "Neutron spectrum unfolding by the Monte-Carlo method," *Nuclear Instruments and Methods in Physics Research Section A: Accelerators, Spectrometers, Detectors and Associated Equipment,* vol. 234, no. 2, pp. 324-330, 1985.

[12] International Organization for Standardization, Reference neutron radiations, part 1: characteristics and methods of production, ISO 8529-1, 2021.
[13] B. C. Cook, J. E. E. Baglin, J. N. Bradford and J. E. Griffin, "$^{12}C(\gamma, n)^{11}C$ Cross-Section to 65 MeV," *Physical Review,* vol. 143, no. 3, 1966.
[14] F. Ajzenberg-Selove, "Energy levels of light nuclei A = 13–15," *Nuclear Physics A,* vol. 523, no. 1, pp. 1-196, 1991.
[15] J. W. Jury, J. S. Hewitt and K. G. McNeill, "Ground state photoneutron angular distributions in the giant resonance of ^{16}O," *Canadian Journal of Physics,* vol. 48, p. 1635, 1970.
[16] B. C. Cook, J. E. E. Baglin, J. N. Bradford and J. E. Griffin, "$^{16}O(\gamma,n)^{15}O$ Cross-Section from Threshold to 65 MeV," *Physical Review,* vol. 143, no. 3, 1966.
[17] R. W. Gellie, K. H. Lokan, N. K. Sherman, R. G. Johnson and J. I. Lodge, "Photoneutron Cross Sections in ^{14}N," *Canadian Journal of Physics,* vol. 50, no. 15, pp. 1689-1696, 1972.
[18] N. K. Sherman, R. W. Gellie, K. H. Lokan and R. G. Johnson, "De-excitation Neutrons Following ^{14}N Photodisintegration," *Phys. Rev. Lett.,* vol. 25, no. 2, pp. 114-116, 1970.
[19] B. L. Berman, S. C. Fultz, J. T. Caldwell, M. A. Kelly and S. S. Dietrich, "Photoneutron Cross-Sections for ^{138}Ba and ^{14}N," *Phys. Rev. C,* vol. 2, no. 6, pp. 2318-2323, 1970.
[20] J. D. King, R. N. H. Haslam and R. W. Parsons, "The gamma-neutron cross-section for 14N," *Canadian Journal of Physics,* vol. 38, no. 2, pp. 231-239, 1960.

406
407